Broad-Band Simultaneous Measurement of Complex Permittivity and Permeability Using a Coaxial Discontinuity

NOUR-EDDINE BELHADJ-TAHAR, ARLETTE FOURRIER-LAMER, AND HÉLIE DE CHANTERAC

Abstract—**A technique is presented for simultaneously measuring the real and imaginary parts of both permittivity and permeability of a given material. A gap in a coaxial line is filled with the material under test. Complex permittivity and permeability are computed from the S-parameter (S_{11} and S_{21}) measurement made on the gap taking into account higher order modes excited at the discontinuity. Measured ϵ_r and μ_r data for several materials are presented from 45 MHz up to 18 GHz. This technique shows good agreement between calculated and generally accepted values.**

I. Introduction

NUMEROUS MEASURING methods applicable to ranges of values for permittivity and permeability and to different frequency bands have been developed by the American Society for Testing and Materials and by various authors [1]–[3]. With the advent of automated vector network analyzers and calculators, broad-band measurements have been developed. Weir [4] uses complex reflection and transmission coefficients presented when a sample of material to be tested is inserted into a waveguide or a transmission line propagating the TEM mode. This method, adopted by Barry [5] in stripline technology, is nevertheless limited in frequency. The increase in frequency in fact is limited by the appearance of resonance phenomena due to the size of the sample and to the presence of higher order modes which are not taken into account in the theoretical formulation of the problem. The method wherein a precision air line is filled with a test specimen is unusual for relatively high ϵ' and μ' (>20) and high frequencies. Sucher [3] shows that air gap errors near inner and outer conductors become increasingly serious with increasing dielectric constant. In the measurement of ceramics in an APC7-mm precision air line ($\epsilon'=10$), for example, the measured ϵ' is about 4.7 for dimensional tolerances of ± 0.01 mm.

The solution presented here uses an inner coaxial conductor discontinuity into which the sample to be measured is easily inserted. The electromagnetic analysis of the structure (direct problem) is valid irrespective of the size of the sample and the working frequency. The uncertainty due to an error in sample dimensions is not a main factor for this method. For this study we used "mode matching," the same method used previously [6] to define the different modes excited by the discontinuity. The calculation of ϵ_r and μ_r from S_{11} and S_{21} measurements (inverse problem) is linked to two infinite systems of simultaneous equations. We demonstrate that this problem is reduced to two systems, each containing three equations with three unknowns. Computer time is therefore reasonable without affecting accuracy.

Manuscript received January 10, 1989; revised July 21, 1989.

The authors are with the Laboraoire de Dispositifs Infrarouge et Microondes, Université Pierre et Marie Curie, 4, Place Jussieu, 75252 Paris Cedex 05, France.

IEEE Log Number 8931552.

II. Direct Problem

A. Formulation of the Problem

We examine the structure shown in Fig. 1. The interruption of the inner conductor of the coaxial line constitutes a circular waveguide filled with a homogeneous and isotropic material. The sample, of thickness $2d$, shows complex permittivity and permeability:

$$\epsilon_r = \epsilon' - j\epsilon'' \tag{1}$$

$$\mu_r = \mu' - j\mu''. \tag{2}$$

The coaxial line is much longer then the transverse dimensions. It is filled with air and propagates the TEM mode only. Moreover the conductors are assumed to be perfect.

At planes $T1$ and $T2$ (the air–material interfaces) the sample can be represented as a quadrupole characterized by its $[Y]$ and $[S]$ matrices [1]. The admittances are normalized in relation to the characteristic admittance of the coaxial line. Given that the structure is symmetrical, the representations used are also symmetrical (Fig. 1). In this case the relationships between the elements of the admittance matrix and those of the scattering matrix are easily obtained:

$$S_{11} = S_{22} = \frac{1 - y_{11}(y_{11} + 2y_{12})}{(1 + y_{11})(1 + y_{11} + 2y_{12})} \tag{3}$$

$$S_{21} = S_{12} = \frac{2y_{12}}{(1 + y_{11})(1 + y_{11} + 2y_{12})}. \tag{4}$$

Let us apply the bisection theorem to the sample and to the quadrupole. In the presence of an electric wall placed

0018-9480/90/0100-0001$01.00 ©1990 IEEE

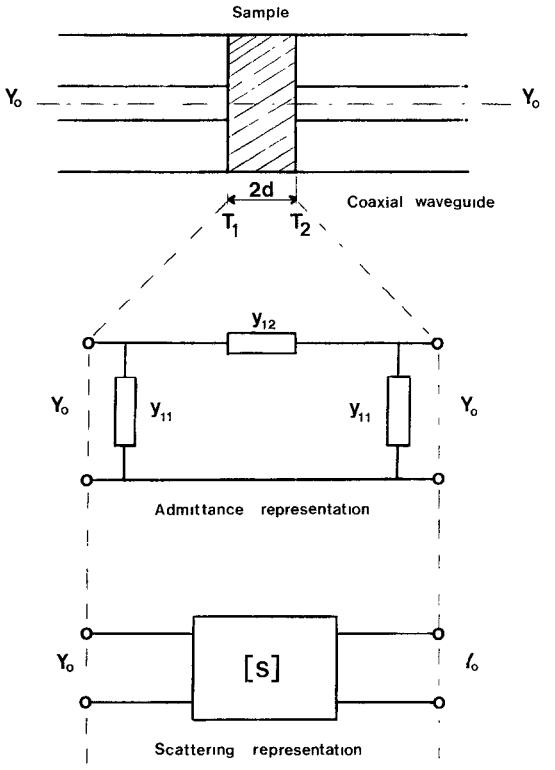

Fig. 1. Geometry of the structure and equivalent representations.

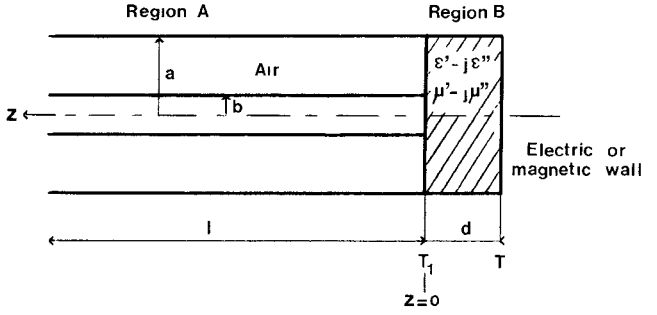

Fig. 2. Representation of the bisected structure.

at plane T, the normalized input admittance at plane $T1$ is

$$y_e = y_{11} + 2y_{12}. \tag{5}$$

If a magnetic wall is next placed at plane T, the input admittance is

$$y_m = y_{11}. \tag{6}$$

As a result, (3) and (4) can be written

$$S_{11} = S_{22} = \frac{1 - y_m y_e}{(1 + y_m)(1 + y_e)} \tag{7}$$

$$S_{21} = S_{12} = \frac{y_e - y_m}{(1 + y_m)(1 + y_e)}. \tag{8}$$

Equations (7) and (8) enable us to link the measurements of the S parameters to the electric and magnetic properties of the material placed in the cell. To calculate the input impedances y_e and y_m we used the same electromagnetic analysis as before [6].

Let us consider a TEM wave propagating in region A of Fig. 2. The cylindrical symmetry enables us to predict that only E modes independent of the azimuthal angle ϕ will be excited at the $z = 0$ plane. To be unhampered by the line excitation method, we take a length of coaxial line which is much longer than the transverse dimensions so that the higher order modes created by the source are not superposed on the higher order modes excited by the discontinuity.

In the air-filled region A, the components of the total electromagnetic field are

$$E_{rA} = \frac{1}{r} A_0 (\exp + jk_0 z + \Gamma \exp - jk_0 z) + \sum_{q=1}^{\infty} A_q Z_1(\zeta_q r) \exp \gamma_q z \tag{9}$$

$$E_{zA} = \sum_{q=1}^{\infty} A_q \frac{\zeta_q}{\gamma_q} Z_0(\zeta_q r) \exp - \gamma_q z \tag{10}$$

$$H_{\phi A} = \frac{1}{r} A_0 Y_{A_0} (\exp + jk_0 z - \Gamma \exp - jk_0 z) + \sum_{q=1}^{\infty} A_q Y_{Aq} Z_1(\zeta_q r) \exp - \gamma_q z \tag{11}$$

where A_0 represents the incidents TEM wave amplitude and Γ its reflection coefficient at plane $T1$ of the discontinuity; Y_{A0} and Y_{Aq} are respectively the wave admittances of the TEM mode and the higher order mode E_{0q} in the coaxial waveguide:

$$Y_{A0} = -\sqrt{\frac{\epsilon_0}{\mu_0}} \tag{12}$$

$$Y_{A_q} = \frac{j\omega\epsilon_0}{\gamma_q} \tag{13}$$

with

$$k_0 = \omega\sqrt{\epsilon_0 \mu_0} \tag{14}$$

and

$$\gamma_q = \sqrt{\zeta_q^2 - k_0^2}. \tag{15}$$

In (9), (10), and (11), Z_p denotes the linear combination of the pth-order Bessel functions of the first and second kinds as follows:

$$Z_p(\zeta_q r) = J_p(\zeta_q r) + G_{Aq} N_p(\zeta_q r) \qquad \text{with } p = 0 \text{ or } 1. \tag{16}$$

When an electric wall is placed at plane T, the electric field boundary conditions at this plane provide the solutions for region B:

$$E_{rB} = \sum_{\iota=1}^{\infty} B_\iota' J_1(\lambda_\iota r) \mathrm{sh}\gamma_\iota (z + d) \tag{17}$$

$$E_{zB} = \sum_{\iota=1}^{\infty} B_\iota' \frac{\lambda_\iota}{\gamma_\iota} J_0(\lambda_\iota r) \mathrm{ch}\gamma_\iota (z + d) \tag{18}$$

$$H_{\phi B} = \sum_{\iota=1}^{\infty} -\frac{j\omega\epsilon_0\epsilon_r}{\gamma_\iota} B_\iota' J_1(\lambda_\iota r) \mathrm{ch}\gamma_\iota (z + d). \tag{19}$$

with

$$\gamma_i = \sqrt{\lambda_i^2 - k^2} \tag{20}$$

and

$$k^2 = k_0^2 \epsilon_r \mu_r. \tag{21}$$

The axial component E_z for the electric field for each E wave must be zero at the conductors in the two regions. The following conditions are thus obtained:

$$Z_0(\zeta_q a) = Z_0(\zeta_q b) = 0 \tag{22}$$

$$J_0(\lambda_i a) = 0. \tag{23}$$

Relation (22) enables us to determine the coefficient G_{Aq} contained in (16):

$$G_{Aq} = -\frac{J_0(\zeta_q a)}{N_0(\zeta_q a)} = -\frac{J_0(\zeta_q b)}{N_0(\zeta_q b)} \tag{24}$$

and thus from the transcendental equation (25), the coefficient ζ_q:

$$J_0(\zeta_q a) N_0(\zeta_q b) - J_0(\zeta_q b) N_0(\zeta_q a) = 0. \tag{25}$$

The matching conditions for the transverse components at the plane T_1 are expressed in the following manner:

$$E_{rB} = 0, \qquad 0 < r < b \tag{26}$$

$$E_{rB} = \sum_{i=1}^{\infty} B_i J_1(\lambda_i r) = \frac{1}{r} A_0 (1+\Gamma) + \sum_{q=1}^{\infty} A_q Z_1(\zeta_q r), \qquad b < r < a \tag{27}$$

$$H_{\phi B} = \sum_{i=1}^{\infty} B_i Y_{ei} J_1(\lambda_i r) = \frac{1}{r} A_0 Y_{A0} (1-\Gamma) + \sum_{q=1}^{\infty} A_q Y_{Aq} Z_1(\zeta_q r), \qquad b < r < a \tag{28}$$

where

$$B_i = B_i' \operatorname{sh} \gamma_i d \tag{29}$$

and

$$Y_{ei} = \frac{-j\omega\epsilon_0\epsilon_r}{(\lambda_i^2 - k^2)^{1/2}} \coth\left(\sqrt{\lambda_i^2 - k^2}\, d\right). \tag{30}$$

Coefficients A_q and B_i are determined by using the orthogonality properties of Bessel functions. The first step is to perform the following integral:

$$\int_0^a r J_1(\lambda_s \cdot r) E_{rB}. \tag{31}$$

Using Lommel integrals and equalities (26), (27), (22), and (23), we obtain

$$\frac{B_i}{\lambda_i} = A_0 (1+\Gamma) \frac{2J_0(\lambda_i b)}{\lambda_i^2 a^2 J_1^2(\lambda_i a)} \cdot \left(1 - \sum_{q=1}^{\infty} \frac{A_q}{A_0(1+\Gamma)} \cdot \frac{bZ_1(\zeta_1 b)}{\zeta_q^2/\lambda_i^2 - 1}\right). \tag{32}$$

Next, $H_{\phi B}$ is integrated over the range $b < r < a$. Relations (28), (22), and (23) give

$$Y_{A_0} A_0 (1-\Gamma) \ln\frac{a}{b} = \sum_{i=1}^{\infty} \frac{B_i Y_{ei}}{\lambda_i} J_0(\lambda_i b). \tag{33}$$

The last step is to integrate the quantity $rZ_1(\zeta_n r) H_{\phi B}$ over the range $b < r < a$. Hence

$$\frac{Y_{An}}{2} A_n b Z_1(\zeta_n b) \left[\frac{a^2 Z_1^2(\zeta_n a)}{b^2 Z_1^2(\zeta_n b)} - 1\right] = \sum_{i=1}^{\infty} \frac{B_i Y_{ei} \lambda_i J_0(\lambda_i b)}{\lambda_i^2 - \zeta_n^2}. \tag{34}$$

The normalized input admittance y_e in the plane T_1 may be written in the following form: $\frac{1-\Gamma}{1+\Gamma}$. Equations (32) and (33) allow us derive the solution:

$$y_e = j \frac{2k_0 a \epsilon_r}{\ln\frac{a}{b}} \sum_{i=1}^{\infty} \frac{J_0^2(\lambda_i b) \coth\left[(\lambda_i^2 a^2 - k^2 a^2)^{1/2} d/a\right]}{(\lambda_i^2 a^2 - k^2 a^2)^{1/2} \lambda_i^2 a^2 J_1^2(\lambda_i a)} \cdot \left(1 - \sum_{q=1}^{\infty} \frac{A_q}{A_0(1+\Gamma)} \cdot \frac{bZ_1(\zeta_q b)}{\zeta_q^2/\lambda_i^2 - 1}\right). \tag{35}$$

or, alternatively,

$$y_e = j \frac{2k_0 a \epsilon_r}{\ln\frac{a}{b}} \left(y_0 - \sum_{q=1}^{\infty} y_q x_q\right) \tag{36}$$

assuming that

$$y_0 = \sum_{i=1}^{\infty} \frac{\coth\left[(\lambda_i^2 a^2 - k^2 a^2)^{1/2} d/a\right]}{(\lambda_i^2 a^2 - k^2 a^2)^{1/2} \lambda_i^2 a^2} \cdot \frac{J_0^2(\lambda_i b)}{J_1^2(\lambda_i a)} \tag{37}$$

$$x_q = \frac{A_q}{A_0(1+\Gamma)} \cdot bZ_1(\zeta_q b) \tag{38}$$

$$y_q = -\sum_{i=1}^{\infty} \frac{\coth\left[(\lambda_i^2 a^2 - k^2 a^2)^{1/2} d/a\right]}{(\lambda_i^2 a^2 - k^2 a^2)^{1/2} (\lambda_i^2 a^2 - \zeta_q^2 a^2)} \cdot \frac{J_0^2(\lambda_i b)}{J_1^2(\lambda_i a)}. \tag{39}$$

The coefficients x_q are obtained from (34) using relations

(32), (30), and (13). This leads to the matrix equation

$$\frac{1}{\epsilon_r}\cdot\frac{x_n}{4\left(\zeta_n^2a^2-k_0^2a^2\right)^{1/2}}\left[\frac{a^2Z_1^2(\zeta_n a)}{b^2Z_1^2(\zeta_n b)}-1\right]$$
$$=\sum_{i=1}^{\infty}-\frac{\coth\left[\left(\lambda_i^2a^2-k^2a^2\right)^{1/2}d/a\right]}{\left(\lambda_i^2a^2-k^2a^2\right)^{1/2}\left(\lambda_i^2a^2-\zeta_n^2a^2\right)}\cdot\frac{J_0^2(\lambda_i b)}{J_1^2(\lambda_i a)}$$
$$-\sum_{i=1}^{\infty}\sum_{q=1}^{\infty}x_q\frac{\lambda_i^2a^2\coth\left[\left(\lambda_i^2a^2-k^2a^2\right)^{1/2}d/a\right]}{\left(\lambda_i^2a^2-k^2a^2\right)^{1/2}\left(\lambda_i^2a^2-\zeta_q^2a^2\right)\left(\lambda_i^2a^2-\zeta_n^2a^2\right)}\cdot\frac{J_0^2(\lambda_i b)}{J_1^2(\lambda_i a)} \tag{40}$$

or

$$\sum_{q=1}^{\infty}A_{qn}x_q=y_n,\qquad n=1,2,\cdots \tag{41}$$

assuming that

$$A_{qn}=\sum_{i=1}^{\infty}\frac{\lambda_i^2a^2\coth\left[\left(\lambda_i^2a^2-k^2a^2\right)^{1/2}d/a\right]}{\left(\lambda_i^2a^2-k^2a^2\right)^{1/2}\left(\lambda_i^2a^2-\zeta_q^2a^2\right)\left(\lambda_i^2a^2-\zeta_n^2a^2\right)}$$
$$\cdot\frac{J_0^2(\lambda_i b)}{J_1^2(\lambda_i a)}+\frac{1}{\epsilon_r}\frac{\delta_{qn}}{4\left(\zeta_n^2a^2-k_0^2a^2\right)^{1/2}}\left[\frac{a^2Z_1^2(\zeta_n a)}{b^2Z_1^2(\zeta_n b)}-1\right] \tag{42}$$

where δ_{qn} is the Kronecker symbol.

If a magnetic wall is placed in the bisection plane T, the total electromagnetic field in region B is

$$E_{rB}=\sum_{i=1}^{\infty}B_i''J_1(\lambda_i r)\operatorname{ch}\gamma_i(z+d) \tag{43}$$

$$E_{zB}=\sum_{i=1}^{\infty}B_i''\frac{\lambda_i}{\gamma_i}J_0(\lambda_i r)\operatorname{sh}\gamma_i(z+d) \tag{44}$$

$$H_{\phi B}=\sum_{i=1}^{\infty}\frac{-j\omega\epsilon_0\epsilon_r}{\gamma_i}B_i''J_1(\lambda_i r)\operatorname{sh}\gamma_i(z+d). \tag{45}$$

At the reference plane T_1 these components can be written as follows:

$$E_{rB}=\sum_{i=1}^{\infty}B_iJ_1(\lambda_i r) \tag{46}$$

$$E_{zB}=\sum_{i=1}^{\infty}B_i\frac{\lambda_i}{\gamma_i}J_0(\lambda_i r)\cdot\operatorname{th}\gamma_i d \tag{47}$$

$$H_{\phi B}=\sum_{i=1}^{\infty}B_iY_{mi}J_1(\lambda_i r) \tag{48}$$

with

$$B_i=B_i''\operatorname{ch}\gamma_i d \tag{49}$$

and

$$Y_{mi}=-j\frac{\omega\epsilon_0\epsilon_r}{\left(\lambda_i^2-k^2\right)^{1/2}}\cdot\operatorname{th}\left[\left(\lambda_i^2-k^2\right)^{1/2}d\right]. \tag{50}$$

Hence the same procedure is adopted to calculate the input admittance y_m. We find the same results in replacing coth( ) with th( ) in (26) to (42):

$$y_m=j\frac{2k_0a\epsilon_r}{\ln\frac{a}{b}}\left(y_0'-\sum_{q=1}^{\infty}y_q'x_q'\right). \tag{51}$$

B. Numerical Computation

The S-parameter computation starts with the evaluation of quantities λ_i and ζ_q from a Bessel subroutine. The roots of the transcendental equations (23) and (25) are found by iteration. It can be shown that all these roots (λ_i and ζ_q) are real, even in the lossy case (lossy materials in region B) and so the arguments of the calculated Bessel functions are real. These functions are programmed in the polynomial approximations from [7] with an absolute accuracy of 10^{-8}. Hence for a given frequency and for a material of known properties, coefficients y_0 and y_1 can be computed in the two cases of electric and magnetic walls if the summation over i is truncated. In fact, this truncation recurs to retaining a finite number of higher order modes excited by the discontinuity and present in the sample ($i=1,2,\cdots,I$). In the same manner, to compute the coefficient A_{qn} we retain Q higher order modes excited in the coaxial waveguide by the discontinuity. Hence (41) is reduced to two systems of Q equations with Q unknowns x_q ($q=1,2,\cdots,Q$). From this, y_e and y_m values are obtained. Since the value of Q governs the number of simultaneous equations to be solved, it is clear that, for a solution of given accuracy, there will be a considerable saving of computer time and storage if the ratio I/Q is correctly chosen. The effect on the admittance computation accuracy of the number of higher order modes retained has been described in [8]. We show that the accuracy is better than 0.1 percent if we take $I=2Q=6$. Investigations on the rate of convergence for different values of I and Q used in the mode-matching method have been reported by other authors [9], [10]. These studies show that the convergence rate of the reflection coefficient is improved when the ratio I/Q corresponds to the ratio of the cross-sectional areas of the waveguides on either side of the junction and that the convergence is sufficient after only three modes in the small waveguide. Hence all our computations are performed with $I=6$ and $Q=3$. An example is depicted in Figs. 3 and 4. Theoretical and measured values of S_{11} and S_{21} are presented between 45 MHz and 18 GHz for an APC7 millimeter cell filled with air ($2d=0.85$ mm).

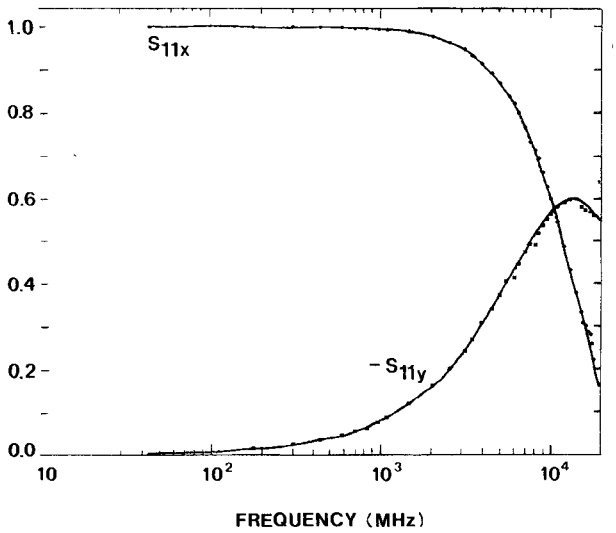

Fig. 3. Real and imaginary parts of the S_{11} parameter for the gap filled with air in APC7 millimeter coaxial waveguide filled with air; $2d = 0.85$ mm. (●) Experimental data. ----- Theoretical data.

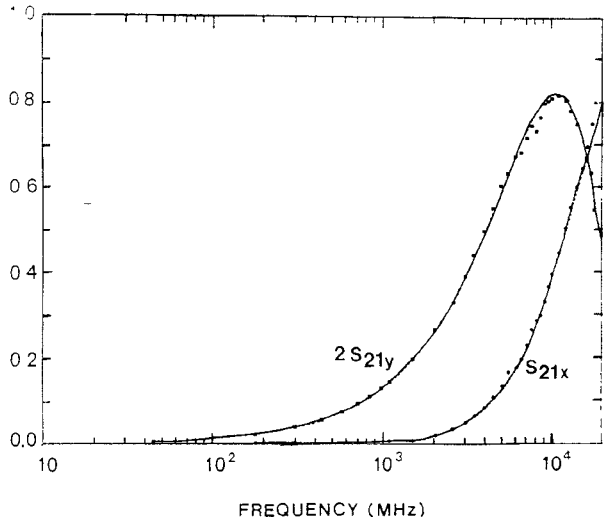

Fig. 4. Real and imaginary parts of the S_{21} parameter for the gap filled with air in APC7 millimeter coaxial waveguide filled with air; $2d = 0.85$ mm. (●) Experimental data. ----- Theoretical data.

III. Inverse Problem

This section involves the complex permittivity and permeability computation from S-parameter measurements of the gap filled by the sample. To avoid contact resistances and contact capacitances, the sample is metallized on the contact surfaces with the line conductors. Numerical computations are performed with the HP 9000 series 300 desktop computer.

The simultaneous classification of $\epsilon_r = \epsilon' - j\epsilon''$ and $\mu_r = \mu' - j\mu''$ is carried out by comparison between measured and calculated S_{11} and S_{21} values. For this purpose we use an iterative method derived from the gradient method. For any initial vector,

$$\vec{C_0} = \begin{bmatrix} \epsilon' \\ \epsilon'' \\ \mu' \\ \mu'' \end{bmatrix} \tag{52}$$

we define an error vector $\Delta\vec{S}$ in the following manner:

$$\Delta\vec{S} = \begin{bmatrix} S_{11x}^{(m)} - S_{11x}^{(c)} \\ S_{11y}^{(m)} - S_{11y}^{(c)} \\ S_{21x}^{(m)} - S_{21x}^{(c)} \\ S_{21y}^{(m)} - S_{21y}^{(c)} \end{bmatrix} \tag{53}$$

where the superscripts m and c denote respectively the measured and calculated S parameters in rectangular coordinates. At the $\Delta\vec{S}$ vector we associated a second vector $\Delta\vec{C}$ as follows:

$$\Delta\vec{S} = [D]\Delta\vec{C} \tag{54}$$

where the matrix $[D]$ is defined as the derivative matrix:

$$[D] = \begin{bmatrix} \frac{\partial S_{11x}}{\partial \epsilon'} & \frac{\partial S_{11x}}{\partial \epsilon''} & \frac{\partial S_{11x}}{\partial \mu'} & \frac{\partial S_{11x}}{\partial \mu''} \\ \frac{\partial S_{11y}}{\partial \epsilon'} & \frac{\partial S_{11y}}{\partial \epsilon''} & \frac{\partial S_{11y}}{\partial \mu'} & \frac{\partial S_{11y}}{\partial \mu''} \\ \frac{\partial S_{21x}}{\partial \epsilon'} & \frac{\partial S_{21x}}{\partial \epsilon''} & \frac{\partial S_{21x}}{\partial \mu'} & \frac{\partial S_{21x}}{\partial \mu''} \\ \frac{\partial S_{21y}}{\partial \epsilon'} & \frac{\partial S_{21y}}{\partial \epsilon''} & \frac{\partial S_{21y}}{\partial \mu'} & \frac{\partial S_{21y}}{\partial \mu''} \end{bmatrix} \tag{55}$$

and

$$\Delta\vec{C} = \begin{bmatrix} \Delta\epsilon' \\ \Delta\epsilon'' \\ \Delta\mu' \\ \Delta\mu'' \end{bmatrix}. \tag{56}$$

The value of the $\Delta\vec{C}$ vector is obtained from the inverse matrix $[D]^{-1}$ as follows:

$$\Delta\vec{C} = [D]^{-1} \cdot \Delta\vec{S}. \tag{57}$$

The new direction of investigation is now

$$\vec{C_n} = \vec{C_{n-1}} + \begin{bmatrix} \alpha_1 \Delta\epsilon' \\ \alpha_2 \Delta\epsilon'' \\ \alpha_3 \Delta\mu' \\ \alpha_4 \Delta\mu'' \end{bmatrix} \tag{58}$$

where the α_i coefficients are equal to 0.8 at maximum. The choice of the coefficients α_i is performed to give fast convergence. The iterations are stopped when $\|\Delta\vec{S}\|^2$ is lower than 10^{-8}. This value is fixed by the accuracy of the network analyzer. The calculated ϵ_r and μ_r values become the initial values for the next measured point. The typical computation time for an experimental frequency point is lower than 1 minute.

IV. Experimental Results

The results of the measurements on Teflon and alumina are represented in Figs. 5, 6, 7, and 8. The measurements performed on each of these materials were obtained at room temperature using the HP 8510A network analyzer in APC7 millimeter standard. The thickness of the Teflon sample was 4.4 mm, and that of the alumina was 4 mm. These two materials show ϵ' values of 2.1 [5] and 9.8 [11]

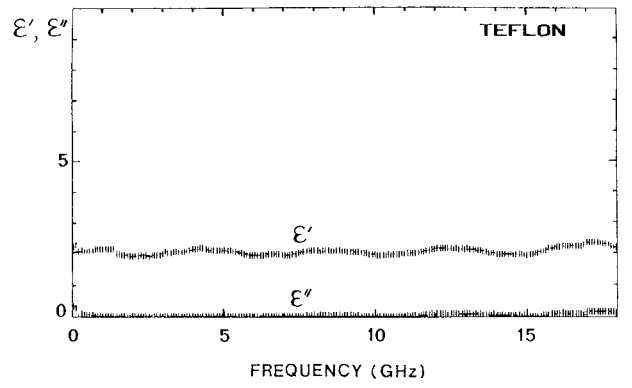

Fig. 5. Complex permittivity measured for a Teflon sample in the 45 MHz–18 GHz frequency range; thickness = 4.4 mm; APC7-mm standard.

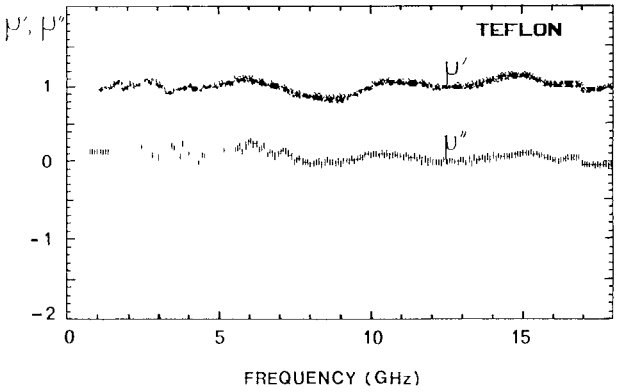

Fig. 6. Complex permeability measured for the Teflon sample in the 45 MHz–18 GHz frequency range; thickness = 4.4 mm; APC7-mm standard.

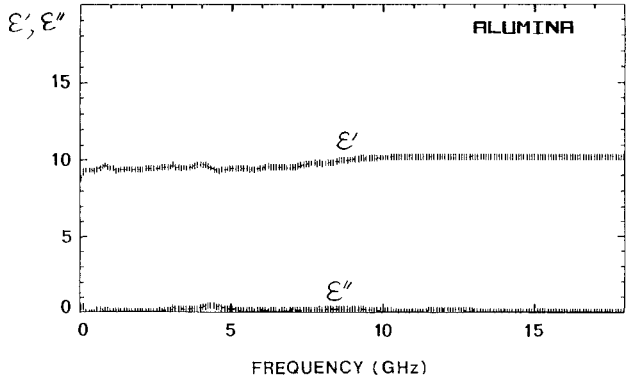

Fig. 7. Complex permittivity measured for an alumina sample in the 45 MHz–18 GHz frequency range; thickness = 4 mm; APC7-mm standard.

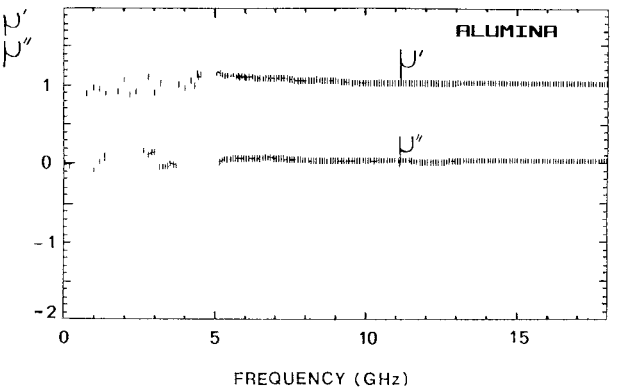

Fig. 8. Complex permeability measured for the alumina sample in the 45 MHz–18 GHz frequency range; thickness = 4 mm; APC7-mm standard.

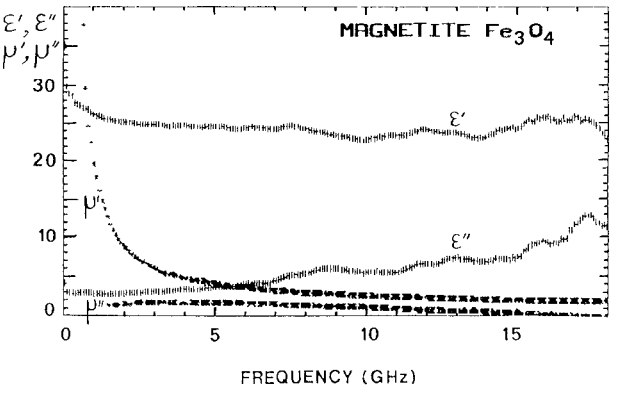

Fig. 9. Complex permittivity and permeability for the magnetite Fe_3O_4. The sample is powder compacted at 3.5 metric tons.

respectively and very low losses (ϵ'' is lower than 0.0004 for Teflon [2] and than 0.001 for alumina). They are nonmagnetic and have a relative permeability of 1. The values measured, depicted in Figs. 5 to 8, correspond to those anticipated. However, because of the large errors in small ϵ'' and μ'', the measurement of low-loss samples is difficult with this technique. To obtain reasonable accuracy. ϵ'' and μ'' should be greater than 0.1. At very low frequencies, the value of μ_r for nonmagnetic materials cannot be evaluated with accuracy due to residual mismatch errors. As one may expect, examination of (35) and (51) shows that μ_r is involved in the difference between $\lambda_i^2 a^2$ and $k^2 a^2$ only, in contrast to ϵ_r, which appears in this difference and as a multiplicative term in (35) and (51). For the very low frequencies, k is smaller than λ_1 and the μ_r measurement for nonmagnetic material becomes difficult. The instrumentation errors depend on the magnitudes of S_{11} and S_{21}. The magnitude and phase errors for S_{11} increase when $|S_{11}|$ approaches zero. The magnitude and phase errors for S_{21} increase when $|S_{21}|$ is lower than 0.1. As $|S_{21}|$ is usually lower than 0.1 for frequencies below 1 GHz, the maximum error for μ_r occurs in this band of frequencies. For Teflon and alumina samples, the length is selected to give S_{11} and S_{21} of equal magnitudes, which achieves greatest accuracy.

The accuracy of the method was computed by simulation on a calculator. The calculator, programmed for the HP8510A system instrumentation errors, and the measurements of the S_{11} and S_{21} values enable the measuring errors in ϵ_r and μ_r to be determined. At the lower end of the frequency range, the permeability accuracy depends on the permittivity values and is better than 10 percent for higher values of ϵ' ($\epsilon' > 5$). This accuracy increases with frequency and the sample thickness and is better than 5 percent above 5 GHz. The permittivity accuracy is practically constant and is equal to 2 percent. The uncertainty

for ϵ_r and μ_r caused by a small error in the physical length of the sample is practically equal to the percentage of the error. As it is easy to measure the sample length to an accuracy within ± 0.01 mm, the uncertainty due to an error in the length of the sample material is not a main factor for this measurement method.

The permittivity and permeability of the magnetite Fe_3O_4 were measured with this technique ($2d = 1$ mm). The sample is powder compacted at a pressure of 3.5 metric tons for one minute. The measurement results appear in Fig. 9.

V. Conclusion: Extending the Method to Millimeter Waves

A broad-band technique is presented for simultaneously measuring the real and imaginary parts of both the permittivity and permeability of a given material. The material under test fills a gap in a coaxial line. To avoid contact resistances and contact capacitances, the sample is metallized on the contact surfaces with the line conductors. Required dimensional tolerances are 0.01 mm. The values of ϵ_r and μ_r are computed from measurements of S_{11} and S_{21} made on an automated network analyzer. This method is easy to use and requires no corrections in experimental results. With a single sample, it allows continuous characterization up to 18 GHz. By using APC2.4 millimeter connections, the method can be extended up to 50 GHz. Consequently magnetic materials can be studied at millimeter wavelengths.

References

[1] P. A. Miles, W. B. Westphal, and A. von Hippel, "Dielectric spectroscopy of ferromagnetic semiconductors," *Rev. Mod. Phys.*, vol. 29, pp. 279–307, July 1957.

[2] A. von Hippel, *Les Dielectriques et leurs Applications*. Paris: Dunod, 1961.

[3] M. Sucher and J. Fox, *Handbook of Microwave Measurements*, 3rd ed. New York: Wiley and Sons, 1963, vol. II.

[4] W. B. Weir, "Automatic measurement of complex dielectric constant and permeability at microwave frequencies," *Proc. IEEE*, vol. 62, pp. 33–36, Jan. 1974.

[5] W. Barry, "A broad-band, automated, stripline technique for the simultaneous measurement of complex permittivity and permeability," *IEEE Trans. Microwave Theory Tech.*, vol. MTT-34, pp. 80–84, Jan. 1986.

[6] N. E. Belhadj-Tahar and A. Fourrier-Lamer, "Broad-band analysis of a coaxial discontinuity used for dielectric measurements," *IEEE Trans. Microwave Theory Tech.*, vol. MTT-34, pp. 346–350, Mar. 1986.

[7] M. Abramowitz and I. A. Stegun, *Handbook of Mathematical Functions*. Washington, DC: Government Printing Office, National Bureau of Standards, ch. 9, sect. 4, pp. 369–370.

[8] N. E. Belhadj-Tahar and A. Fourrier-Lamer, "Utilisation Pratique d'une Cellule Très Large Bande pour la Mesure Automatique de la Permittivité de Divers Matèriaux," *Onde Elec.*, vol. 68, pp. 50–59, Jan. 1988.

[9] P. H. Masterman and P. J. B. Clarricoats, "Computer field-matching solution of waveguide transverse discontinuities," *Proc. Inst. Elec. Eng.*, vol. 118, pp. 51–63, Jan. 1971.

[10] W. J. English, "The circular waveguide step-discontinuity mode transducer," *IEEE Trans. Microwave Theory Tech.*, vol. MTT-21, pp. 633–636, Oct. 1973.

[11] J. H. C. van Heuven and T. H. A. M. Vlek, "Anisotropy in alumina substrates for microstrip circuits," *IEEE Trans. Microwave Theory Tech.*, vol. MTT-20, pp. 775–777, Nov. 1972.

Nour-Eddine Belhadj-Tahar was born in Tlemcen, Algeria, on September 23, 1954. He received the Dipl.-Ing. degree in electrical engineering from the University of Sciences and Technology of Oran, Algeria, in 1977, and the Ph.D. degree (Doctorat de l'Université Pierre et Marie Curie) in electrical engineering from the University Pierre et Marie Currie, PARIS VI, in 1986.

From 1980 to 1982, he was with the Institute of Physics, University of Tlemcen, Algeria, where he held the position of Assistant Professor. In 1983, he joined the University Pierre et Marie Curie, PARIS VI, where he is presently Assistant Professor. His research activities have been concerned with electromagnetic wave propagation and the analysis of methods for microwave and millimeter-wave dielectric measurement techniques.

Arlette Fourrier-Lamer is Professor of Electronic Engineering at the University of PARIS VI, Pierre et Marie Curie. She received the Ph.D. (Doctorat d'Etat es Sciences Physiques) in 1981. Up to this date, she was engaged in research on electronic and nuclear double resonance (ENDOR) in paramagnetic liquids. Since 1982 she has been working on electromagnetic discontinuities and applications to materials characterization (resins, conducting polymers, superconductors, and ferrites).

Dr. Fourrier-Lamer is a member of the Société Française des Electroniciens et des Radioélectriciens (SEE).

Hélie de Chanterac was born in Cholet, France, in November 1961. He obtained the Diplôme d'Etudes Approfondies (DEA) in microwaves and optoelectronics at the University Pierre et Marie Curie of Paris. Currently, he is working toward the Ph.D. degree (Doctorat de l'Université Pierre et Marie Curie) in electrical engineering. His main areas of interest concern microwave absorbing polymers and systems.